

Room temperature current modulation in large area electronic junctions of spin crossover thin films

Victoria Shalabaeva¹, Karl Ridier¹, Sylvain Rat¹, Maria D. Manrique-Juarez¹, Lionel Salmon¹, Isabelle Séguy², Aurelian Rotaru³, Gábor Molnár^{1,a)}, Azzedine Bousseksou^{1,a)}

¹LCC, CNRS and Université de Toulouse, UPS, INP, F-31077 Toulouse, France.

²LAAS, CNRS and Université de Toulouse, INSA, UPS, F-31077 Toulouse, France.

³Faculty of Electrical Engineering and Computer Science & MANSiD Research Center, Stefan cel Mare University, 13, Str. Universitatii, Suceava 720229, Romania.

^{a)}gabor.molnar@lcc-toulouse.fr and azzedine.bousseksou@lcc-toulouse.fr.

We report large-area ($\sim 3 \text{ mm}^2$), pinhole free crossbar junctions of thin films of the molecular complex $[\text{Fe}(\text{HB}(\text{tz})_3)_2]$ displaying spin transition around 336 K. The charge transport in the thinner junctions (10 and 30 nm) occurs by a tunneling mechanism, which is not affected substantially by the spin transition. The thicker junctions (100 and 200 nm) exhibit rectifying behavior and a reproducible drop of their electrical resistance by *ca.* 65 – 80 % when switching the molecules from the high-spin to the low-spin state. This current modulation is ascribed to a bulk-limited charge transport mechanism *via* a thermally activated hopping process. The demonstrated possibility of resistance switching in ambient conditions provides appealing prospects for the implementation of molecular spin crossover materials in electronic and spintronic devices.

Spin-crossover (SCO) molecular materials are well known to exhibit reversible switching between their low-spin (LS) and high-spin (HS) electronic configurations.¹⁻³ The transition between the two spin states can be triggered by various external stimuli such as temperature, pressure, light irradiation, intense magnetic field as well as the inclusion of guest molecules, and causes significant changes of magnetic, mechanical, optical and electrical properties. The recent spectacular progress in the nanoscale synthesis and organization of SCO materials allowed their integration into different types of electronic junctions with the aim to explore their possible implementation in electronic and spintronic applications.⁴⁻⁷ Notably, voltage-bias induced resistance switching, Kondo switching, memristive properties, spin-polarized current switching phenomena were reported for single SCO molecule junctions,⁸⁻¹⁴ while SCO nanoparticles and thin films were used to construct a range of different resistance switching devices.¹⁵⁻²⁰

Driven by the aim to better understand the physical mechanisms, which couple the spin state of the molecules with the device electrical resistance, some of us recently reported on large-area crossbar devices with nanometric spacer layers of the SCO compound $[\text{Fe}(\text{H}_2\text{B}(\text{pz})_2)_2(\text{phen})]$ (pz

= pyrazol-1-yl and phen = 1,10-phenanthroline) **1** between ITO (indium tin oxide) and Al electrodes.²⁰ This approach provided a robust and well-reproducible way to investigate the current intensity switching, which accompanies the SCO in **1**. As thin films of **1** exhibit a very gradual thermal spin conversion between *ca.* 100-200 K, an unambiguous SCO-induced (*i.e.* non-thermal) variation of the electrical resistance in the junctions could be detected only at low temperatures (5 K), by switching the spin state of the molecules using light irradiation. In particular, the ITO/**1**/Al junctions with 10 nm thick SCO films showed an activationless, multi-step tunneling conductivity, while the 30 and 100 nm thick junctions exhibited thermally activated, bulk transport-limited currents with a diode-like rectifying behavior. The optical switching from the LS to the HS state led to a well reproducible decrease of the current intensity by ~7 % and ~50 % for the 10 and 30 nm junctions, respectively, which was attributed to the reduced hopping rate of charge carriers in the HS state.

In this Letter, we extend this investigation to thin films of another SCO complex [Fe(HB(tz)₃)₂] (tz = triazol-1-yl) **2**, which displays SCO around room temperature. Through this study we intend to examine: (i) if the current modulation can be also observed at technologically more relevant temperatures (*i.e.* near room temperature), (ii) if the large-area junctions of **1**, which is an amorphous material, can be also reproduced using polycrystalline SCO films, which is the case of **2** and (iii) if the charge transport mechanisms as well as their spin-state dependence observed in the ITO/**1**/Al junctions are general features for SCO materials.

High-quality, smooth and continuous thin films of **2** can be obtained by vacuum thermal evaporation, followed by solvent-vapor annealing.²¹ The resulting nanocrystalline films are oriented (crystallites grow with the orthorhombic c-axis normal to the surface²¹) and display a fully complete, abrupt and well reproducible first-order spin transition centered at *ca.* 336-339 K. (*N.B.* The spin transition temperature is weakly thickness dependent.²²) The films are robust and stable both on thermal cycling (up to at least 100 °C) and upon storage in ambient air (up to at least a year). For the present study thin films were grown by thermal evaporation at 170 °C under high vacuum (2×10^{-7} mbar) at a rate of 0.3 \AA s^{-1} on 180 nm thick, lithographically patterned ITO electrodes (on glass substrates). The as-deposited amorphous films were recrystallized in *ca.* 80 % relative humidity air at room temperature for 10 min. The 100 nm thick upper Al electrodes were finally thermally evaporated through a shadow mask with a rate of 10 \AA s^{-1} . During the evaporation of the Al film, the device was cooled by water to prevent the perforation of the SCO layer. As a result, each device consists of six crossbar ITO/**2**/Al stacks with an effective junction area of *ca.* 3 mm^2 each (see [Figure 1a](#)).

[Figure 1b](#) depicts a representative AFM topography image of the SCO film showing a smooth and continuous surface coverage. The film thickness was monitored *in-situ* during the growth by a quartz crystal microbalance and confirmed by scanning electron microscopy (SEM) analyses on the junction cross-sections, following focused ion beam (FIB) milling (see [Figure 1c](#)). Four different junctions with nominal thicknesses of 10, 30, 100 and 200 nm were fabricated. One of the key advantages of these large area devices is that the SCO properties of the junctions can be

determined by straightforward optical methods parallel to the electrical measurements. The spin transition in the junction area was confirmed by optical reflectivity measurements (see [Figure S1](#) in [supplementary material](#)). A more quantitative UV absorption analysis of the films was also conducted using a spectrophotometer (Cary 50, Agilent Technologies) and a heating-cooling chamber (Linkam FTIR-600). [Figure 1d](#) shows the temperature dependence of the absorbance of the films at 317 nm recorded in the 293-383 K range with $\pm 5 \text{ Kmin}^{-1}$ scan rates. Clear changes are observed in the absorbance of the 30, 100 and 200 nm thick films at the thermal spin transition temperature (*ca.* 336 - 339 K), which are proportional to the junction thickness. However, for the 10 nm junctions it was not possible to detect the spin transition, presumably due to the very small thickness of the films.

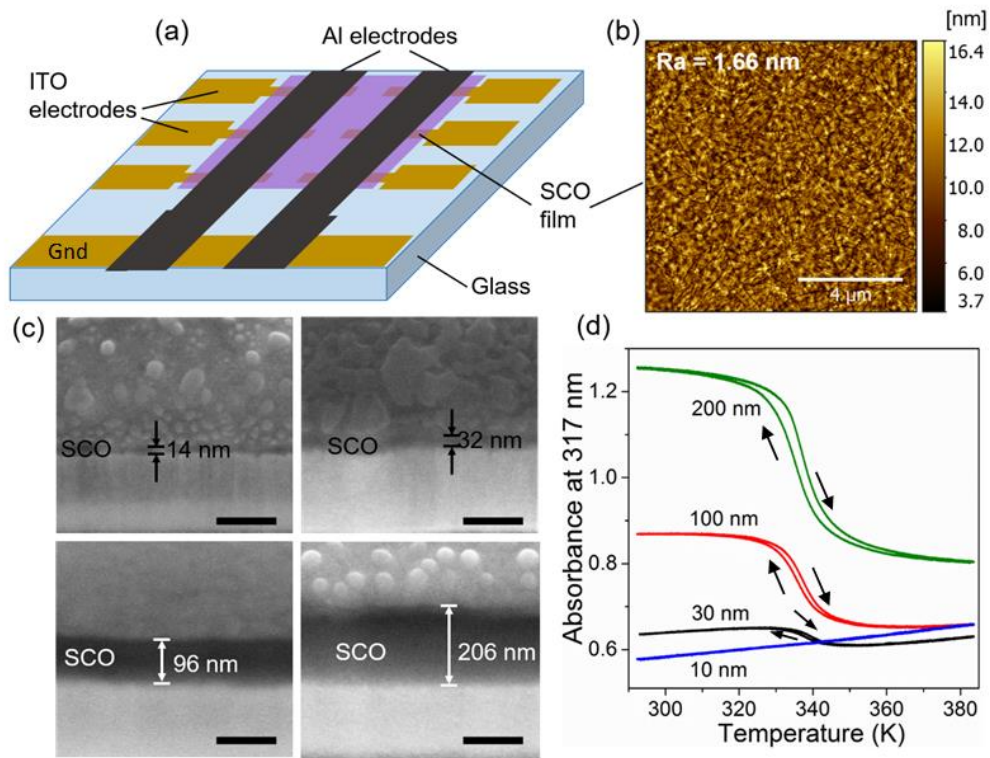


FIG 1. (a) Scheme of the device structure representing six crossbar junctions of ITO/2/Al stacks. (b) AFM topography image of the 30 nm SCO film deposited on the ITO surface. R_a is the arithmetic mean roughness. (c) SEM images of FIB milled cross-sections of the junctions with different SCO thicknesses. (d) Temperature dependence of the UV absorbance of the SCO films at $\lambda = 317 \text{ nm}$. Arrows show the heating and cooling branches of the hysteresis

Current – voltage (I - V) and current – temperature (I - T) characteristics of the junctions were analyzed under ambient air in two-probe mode using a Keithley-6430 source-meter and a heating-cooling stage (Linkam HFS600-P) equipped with gold-tipped tungsten probes. For each film thickness we were able to obtain junctions with no sign of contributions from short-circuit channels. This is particularly remarkable in the case of the thinnest (10 nm) films, which tend to form islands on other substrates.²¹ On the average *ca.* 80 % of the fabricated junctions showed reproducible room temperature resistance values with a standard deviation of *ca.* 30 % (for a

given thickness). For each thickness two junctions were then investigated over 3-4 successive thermal cycles. **Figure 2** summarizes the typical results obtained on the 10 and 30 nm thick junctions. The I - V curves are centrosymmetric and fit well the relationship $I = I_0(V + \gamma V^3)$, i.e. the Simmons' intermediate-voltage range tunneling equation²³ (see **Figures S2** and **S3** in the **supplementary material**). Hence the differential conductance dI/dV curves feature a parabolic shape. The Fowler-Nordheim representation ($\ln(I/V^2)$ vs. I/V) of the data for the 10 nm junction leads to a transition voltage, $V_{trans} = 0.6$ V, corresponding to the bias where the tunneling mechanism changes to field emission.²⁴ As such, V_{trans} is conceptually a rough estimation of the tunneling barrier height.

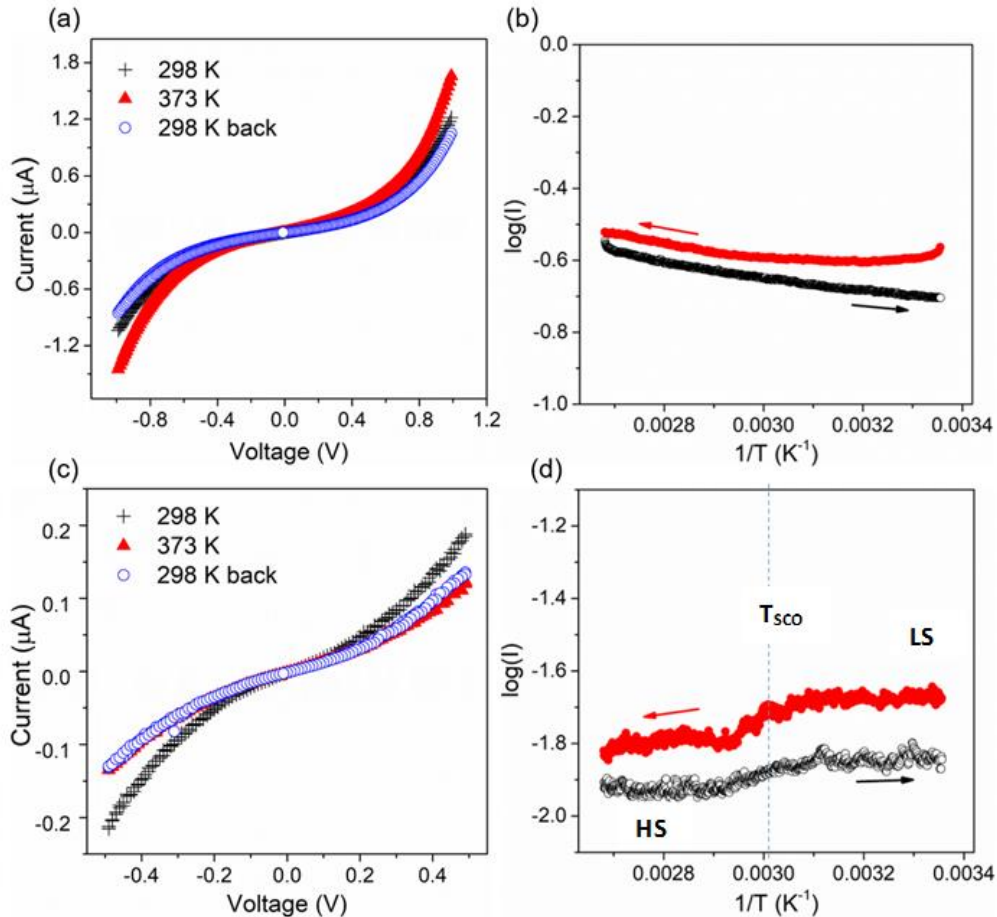


FIG. 2. Typical electrical characteristics of 10 and 30 nm junctions. I - V curves of 10 nm (a) and 30 nm (c) thick junctions recorded at 298, 373 K and then back to 298 K at a scan rate of 10 mVs^{-1} . $\log I$ vs. $1/T$ curves of 10 nm (b) and 30 nm (d) thick junctions recorded with an applied bias of 0.5 V and 0.3 V, respectively, at a scan rate of 5 Kmin^{-1} . Arrows indicate heating and cooling. The dashed line shows the spin transition temperature (T_{sco}).

Figure 2b shows the temperature dependence of the current intensity crossing the 10 nm junction at a constant bias of 0.5 V. No significant temperature effect is observed in the 298 – 373 K range confirming the tunneling nature of the charge transport. This result parallels also the temperature dependence of the UV absorbance in this junction, *i.e.* no effect is detected on the

device characteristics in the SCO temperature region. However, it is difficult to infer a clear conclusion as we cannot be sure if the 10 nm junction exhibits SCO or not. The I - T characteristics of the junction with a 30 nm SCO layer (Figure 2d) show also very weak temperature dependence between 298 and 373 K - in agreement with a tunneling mechanism. On the other hand, these junctions exhibit a small (~10 %) current decrease at *ca.* 336 K. Since this effect was observed in several junctions of the same thickness we attribute it to the thermal spin transition. Here, the conclusion is clear: the 30-nm junctions do exhibit SCO, but this implies only a feeble change of the device resistance.

The electrical characteristics of the 100 and 200 nm thick junctions are summarized in Figure 3. As it can be expected, the thicker devices exhibit a different charge transport behavior. In both devices, the I - V characteristics display a rectifying behavior, which can be fitted by the Shockley diode equation²⁵ (see Figures S4 and S5 in the supplementary material). However, it turned out that under reverse bias conditions the junctions tend to deteriorate and exhibit a progressive decrease of the current intensity - especially at higher temperatures. For this reason Figure 3 shows temperature dependent data acquired exclusively under forward bias conditions (*i.e.* positive bias on the Al electrode) for which the measurements were reproducible. At present we have no clear explanation for this instability under reverse bias and further experiments in inert atmosphere will be necessary to examine the possible role of atmospheric oxygen and water. The I - T curves of the 100 and 200 nm devices reveal a clear thermally activated process since the electrical conductance of the junctions at a constant bias tends to increase with temperature (Figures 3b and 3d). Remarkably, a substantial and reversible change of the current is observed around 336 K. This reversible switching of the electrical resistance is undoubtedly correlated with the spin-state change of the SCO film. The resistance change associated with the spin transition is 80 % and 65 % for the 100 and 200 nm thick junctions, respectively. This effect has been observed in a reproducible manner upon successive thermal cycles and in each investigated junction (see Figure S6 in the supplementary material for further details). Plotting the current density as a function of the applied field reveals a dependence on the junction thickness, which indicates likely a bulk-limited charge transport mechanism (see Figure S3c).²⁶

It is instructive to compare the characteristics of the present ITO/2/Al junctions with those of ITO/1/Al, reported previously in ref. 20. The charge transport in thin junctions is dominated by tunneling in both samples. This process does not correspond to direct tunneling from one electrode to the other, but rather to multiple tunneling steps via localized states in the SCO layer. In this tunneling regime, the effect of the spin transition on the junction resistance appears rather small for both compounds (< 10 %). We have not yet found a satisfactory explanation for this weak spin-state dependence, but it is possibly linked to the specific properties of a small number conducting channels.²⁷ For increasing junction thickness there is a crossover in the dominant charge transport mechanism from tunneling to a bulk-like, thermally-activated hopping process. Interestingly, this crossover occurs in different thickness ranges for the two samples: between 10-30 nm for **1** and 30 -100 nm for **2**, possibly due to their different intrinsic conductivity.

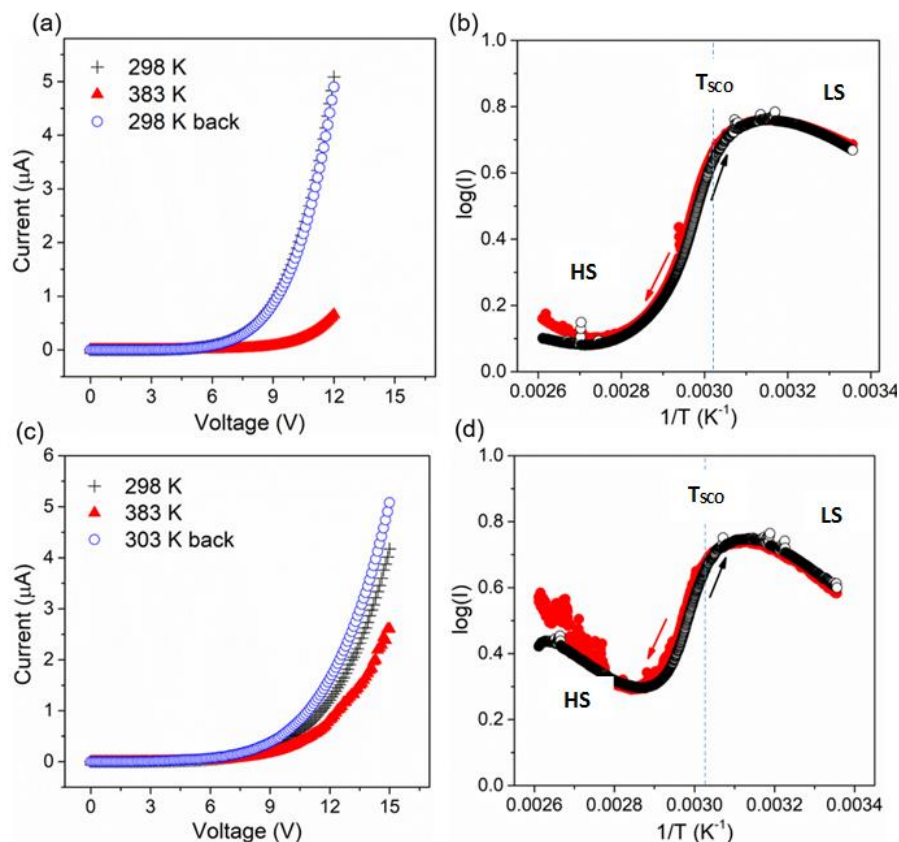


FIG. 3. Typical electrical characteristics of 100 and 200 nm junctions. I - V curves of 100 nm (a) and 200 nm (c) thick junctions recorded at 298, 383 K and then back to 298/303 K at a scan rate of 100 mVs^{-1} . $\log I$ vs. $1/T$ curves of 100 nm (b) and 200 nm (d) thick junctions recorded with an applied bias of 12 V and 15 V, respectively, at a scan rate of 5 Kmin^{-1} . The dashed line shows the spin transition temperature (T_{SCO}).

The I - V curves in the bulk-like regime become asymmetric, which reflects simply the asymmetry of the junctions and thus different interface barriers for charge injection. In this transport regime the junction resistance increases substantially when going from the LS to the HS state (*ca.* 50 % for **1** and *ca.* 65-80 % for **2**). This increase is comparable in magnitude with that observed for the bulk sample of **2** (see Figure S7 in the supplementary material). As discussed in ref. 28, the bulk conductivity of SCO samples is governed by the spin-state dependence of the hopping rate, which is thought to be altered upon the SCO primarily due to the change of phonon frequencies and intermolecular distances. In particular, the lower phonon frequencies and, as a consequence, the lower transmission coefficients can explain the lower conductivity in the HS state. Up to now, the magnitude of the conductivity change between the two spin states was reported relatively low (*ca.* 1-2 orders of magnitude), depending on the compounds and also on their preparation.⁷ Further work should therefore address the possibility to enhance the ON-OFF switching ratios through appropriate material and device design.⁴

In summary, large-area, robust crossbar devices were fabricated by thermal evaporation of the $[\text{Fe}(\text{HB}(\text{tz})_3)_2]$ spin crossover compound in-between ITO and Al electrodes. The comparison

with previous work on the related compound [Fe(H₂B(pz)₂)₂(phen)] gives a consistent picture of the charge transport mechanisms for different junction thicknesses and spin states. Notably, the variable-temperature current-voltage measurements revealed a reproducible jump of the device resistance near room temperature as a consequence of the spin transition in the films. We believe that this property might be useful for further integration of spin-crossover complexes as building blocks in electronic and spintronic devices.

See [supplementary material](#) for additional optical and electrical measurement data.

This work was supported by the Federal University of Toulouse through the project IDEX Emergence NEMSCOOP (ANR-11-IDEX-0002-02), by the Région Occitanie (Contract No. 15050450), by the CNCS-UEFISCDI (project number PN-II-RU-TE-2014-4-2695, Contract No. 267/01.10.2015) and by the European Commission through the SPINSWITCH project (H2020-MSCA-RISE-2016, Grant Agreement No. 734322). The PhD grants of SR and MDMJ were financed, respectively, by the French Ministry of Research and the CONACYT (no. 382038).

¹*Topics in Current Chemistry. Spin Crossover in Transition Metal Compounds*, edited by P. Gütllich and H. A. Goodwin (Springer-Verlag, 2004).

²A. Bousseksou, G. Molnár, L. Salmon and W. Nicolazzi, *Chem. Soc. Rev.* **40**, 3313 (2011).

³*Spin-Crossover Materials: Properties and Applications*, edited by M. A. Halcrow (J. Wiley and Sons, 2013).

⁴G. Molnar, S. Rat, L. Salmon, W. Nicolazzi and A. Bousseksou, *Adv. Mater.* (2017) in press, DOI: 10.1002/adma.201703862.

⁵E. Ruiz, *Phys. Chem. Chem. Phys.* **16**, 14 (2014).

⁶M. Gruber, T. Miyamachi, V. Davesne, M. Bowen, S. Boukari, W. Wulfhekel, M. Alouani and E. Beaupaire, *J. Chem. Phys.* **146**, 092312 (2017).

⁷C. Lefter, V. Davesne, L. Salmon, G. Molnár, P. Demont, A. Rotaru and A. Bousseksou, *Magnetochem.* **2**, 18 (2016).

⁸E. A. Osorio, K. Moth-Poulsen, H. S. J. van der Zant, J. Paaske, P. Hedegård, K. Flensberg, J. Bendix, T. Bjørnholm, *Nano Lett.* **10**, 105 (2010).

⁹T. G. Gopakumar, F. Matino, H. Naggert, A. Bannwarth, F. Tucek and R. Berndt, *Angew. Chem. Int. Ed.* **51**, 6262 (2012).

¹⁰T. Miyamachi, M. Gruber, V. Davesne, M. Bowen, S. Boukari, L. Joly, F. Scheurer, G. Rogez, T. K. Yamada, P. Ohresser, E. Beaupaire and W. Wulfhekel, *Nat. Commun.* **3**, 938 (2012).

¹¹E. J. Devid, P. N. Martinho, M. V. Kamalakar, I. Šalitroš, Ú. Prendergast, J.-F. Dayen, V. Meded, T. Lemma, R. González-Prieto, F. Evers, T. E. Keyes, M. Ruben, B. Doudin and S. J. van der Molen, *ACS Nano* **9**, 4496 (2015).

¹²K. Bairagi, O. Iasco, A. Bellec, A. Kartsev, D. Li, J. Lagoute, C. Chacon, Y. Girard, S. Rousset, F. Miserque, Y. J. Dappe, A. Smogunov, C. Barreteau, M.-L. Boillot, T. Mallah and V.

Repain, [Nat. Commun.](#) **7**, 12212 (2016).

¹³A. C. Aragonès, D. Aravena, J. I. Cerdá, Z. Acís-Castillo, H. Li, J. A. Real, F. Sanz, J. Hihath, E. Ruiz and I. Díez-Pérez, [Nano Lett.](#) **16**, 218 (2016).

¹⁴A. C. Aragonès, D. Aravena, F. J. Valverde-Muñoz, J. A. Real, F. Sanz, I. Díez-Pérez and E. Ruiz, [J. Am. Chem. Soc.](#) **139**, 5768 (2017).

¹⁵M. Matsuda, H. Isozaki and H. Tajima, [Chem. Lett.](#) **37**, 374 (2008).

¹⁶S. Shi, G. Schmerber, J. Arabski, J.-B. Beaufrand, D. J. Kim, S. Boukari, M. Bowen, N. T. Kemp, N. Viart, G. Rogez, E. Beaurepaire, H. Aubriet, J. Petersen, C. Becker and D. Ruch, [Appl. Phys. Lett.](#) **95**, 043303 (2009).

¹⁷T. Mahfoud, G. Molnár, S. Cobo, L. Salmon, C. Thibault, C. Vieu, P. Demont and A. Bousseksou, [Appl. Phys. Lett.](#) **99**, 053307 (2011).

¹⁸F. Prins, M. Monrabal-Capilla, E. A. Osorio, E. Coronado and H. S. J. van der Zant, [Adv. Mater.](#) **23**, 1545 (2011).

¹⁹A. Rotaru, J. Dugay, R. P. Tan, I. A. Gural'skiy, L. Salmon, P. Demont, J. Carrey, G. Molnár, M. Respaud and A. Bousseksou, [Adv. Mater.](#) **25**, 1745 (2013).

²⁰C. Lefter, S. Rat, J. S. Costa, M.D. Manrique-Juarez, C. M. Quintero, L. Salmon, I. Séguy, T. Leichle, L. Nicu, P. Demont, A. Rotaru, G. Molnar and A. Bousseksou, [Adv. Mater.](#) **28**, 7508 (2016).

²¹V. Shalabaeva, S. Rat, M. D. Manrique-Juarez, A. Bas, L. Vendier, L. Salmon, G. Molnar and A. Bousseksou, [J. Mater. Chem. C](#) **5**, 4419 (2017).

²²V. Shalabaeva, M. Mikolasek, M.D. Manrique-Juarez, A.-C. Bas, S. Rat, L. Salmon, W. Nicolazzi, G. Molnár and A. Bousseksou, [J. Phys. Chem. C](#) **121**, 25617 (2017).

²³J. G. Simmons, [J. Appl. Phys.](#) **34**, 1793 (1963).

²⁴R. H. Fowler and L. Nordheim, [Proc. Royal. Soc. A](#) **119**, 173 (1928).

²⁵W. Shockley, [Bell Labs Techn. J.](#) **28**, 435 (1949).

²⁶M. A. Baldo and S. R. Forrest, [Phys. Rev. B](#) **64**, 085201 (2001).

²⁷Y. Xu, D. Ephron and M.R. Beasley, [Phys. Rev. B](#) **52**, 2843 (1995).

²⁸C. Lefter, I. A. Gural'skiy, H. Peng, G. Molnár, L. Salmon, A. Rotaru, A. Bousseksou and P. Demont, [Phys. Stat. Sol. RRL](#) **8**, 191 (2014).